Groundwater and potentially toxic elements in a dismissed mining area: Thallium contamination of drinking spring water in the Apuan Alps (Tuscany, Italy)

Lisa Ghezzi[a,*], Massimo D'Orazio[a], Marco Doveri[b], Matteo Lelli[b], Riccardo Petrini[a], Roberto Giannecchini[a]

[a] Dipartimento di Scienze della Terra, Università di Pisa, via S. Maria 53, I-56126 Pisa, Italy
[b] IGG-CNR, via G. Moruzzi 1, I-56124 Pisa, Italy

ABSTRACT

Thallium is among the most toxic elements to humans. Environmental regulations of the European Community adopted by Italy pose a maximum concentration level for Tl in groundwater of 2 μg/L. However, at present drinkable water must not abide any concentration threshold for thallium and this element is not routinely monitored. In the past-mining area nearby the Valdicastello Carducci village (northern Tuscany, Italy), characterized by Tl-bearing ores, water from a spring that has been tapped for human consumption contains thallium in the range 4.3–27.8 μg/L. The challenge of this study is to highlight the mechanisms leading to Tl contamination in groundwater, by crossing hydrochemical and O-H isotopic data with hydrogeological information. We propose that the Tl-contamination in the spring results from a binary mixing that occurs within a karst system involving an uncontaminated Ca-HCO$_3$ water (mainly interacting with limestone) and a component originated by the interaction of acid drainages (generated by the weathering of Tl-bearing mineral phases in the area) with dolomitic host rocks. In this process, most of the potentially toxic elements released during the weathering are scavenged by the carbonate neutralization of the acid plume due to adsorption onto the iron and manganese oxyhydroxides that formed during pH changes. Nevertheless, the aquifer has little or no attenuation capacity for thallium. Moreover, O-H isotopic data and hydrogeological constraints are compatible with a spring feeding mechanism related to a piston displacement effect.

1. Introduction

Providing safe drinking water for human consumption in public water systems through regulated water sources is of great health concern (WHO, 2017). Among the threats linking the environment to human health, the potentially toxic element (PTE) contamination of drinking waters through natural and/or anthropogenic sources and processes is of raising concern (Chowdhury et al., 2016), also considering the increasing multiple uses of PTE in industrial activities (Tchounwou et al., 2012). Drinking waters mainly derive from groundwater resources (Zhu and Balke, 2008; Baoxiang and Fanhai, 2011) in which the PTE transport can be characterized by complex mechanisms (Siegel, 2002). Indeed, in the European Countries the groundwater exploitation provides water for human consumption for 70% of the population on average (Martınez Navarrete et al., 2008). Even if a number of studies deal with the origin of PTE in drinking

waters, only few investigations so far focus on the contamination of drinking water by thallium (Tl) (Peter and Viraraghavan, 2005; Biagioni et al., 2017), despite this element is of the uppermost public health concern due to its high toxicity to humans (Peter and Viraraghavan, 2005; Rickwood et al., 2015; Colombaioni et al., 2017). European Community poses a maximum Tl concentration level in groundwater of 2 μg/L; nevertheless, at present, Tl is not requested to be surveyed in water intended for human consumption. Because of lack of obligations for chemical testing, it is possible that Tl-contaminated spring water may be used for the distribution systems, inducing health effects that may remain undiscovered for long time.

The exploitation of mineral resources is among the most important activities responsible for the release of PTE to the environment (Nordstrom, 2011; Cidu et al., 2009) including Tl (Casiot et al., 2011; Petrini et al., 2016): the production of acid mine drainages increases metal solubility, and the mineral weathering of mine waste-rock piles

may contaminate draining waters (Jamleson, 2011). In the abandoned mining district of southern Apuan Alps (NW Tuscany, Italy), a densely populated area with a strong touristic vocation, the widespread presence of Tl in ore deposits has been recognized since 2013 (Biagioni et al., 2013). Further studies revealed that Tl concentration can reach about 1000 mg/kg in pyrite ores (D'Orazio et al., 2017) and about 1000 μg/L in acid mine ponds and drainages (Perotti et al., 2017). In this setting, water from a natural spring (named Molini di Sant' Anna, hereafter MSA) outflowing within the Mt. Arsiccio mining area (Perotti et al., 2017) was used as a primary source for public drinking water since the 50s of 1900, and in September 2014 it was discovered to be Tl-contaminated. From that time the spring was excluded from the drinkable water distribution system. However, residents drank Tl-bearing waters for several years without knowing it. A high concentration in urine compared to unexposed population and a significant accumulation in hair was discovered in people living in this settlement (Campanella et al., 2016). "Furthermore, it was observed that Tl became entrapped within pipeline scales during the years, thus yielding a secondary source of contamination that continues to release Tl (Biagioni et al., 2017; Campanella et al., 2017) even after the spring has been excluded from the distribution system.

The aim of the present work was to investigate the mechanism of Tl contamination and propagation in the complex aquifer system drained by the MSA spring.

2. Geological and hydrogeological setting

The study area is located in the southern part of the Apuan Alps (northwestern Tuscany, Italy), and is included within the drainage basin of the Baccatoio Stream (Fig. 1a). The latter is a small water course characterized by an extremely variable regime, and flowing for about 11 km from the mountain range to the Ligurian Sea.

The rocks cropping out in the Apuan Alps area belong to several tectonic-stratigraphic units involved in the Northern Apennines nappe stack (Carmignani and Kligfield, 1990; Conti et al., 1993; Molli and Meccheri, 2012, and references therein). The lower units, which form the metamorphic core complex, are the Apuane and Massa units. These are overlaid by non-metamorphic units (Tuscan Nappe and Ligurian units) and the Neogene to Quaternary sediments. In the upstream zone, the Baccatoio basin includes a small tectonic window exposing rocks of the Paleozoic basement (mostly formed of phyllite, quartzite and metarhyolite) and carbonatic rocks mainly represented by metadolostone (*Grezzoni Fm.*) and marble (*Marmi* Fm.) (Fig. 1b). Such lithologies are unconformably covered by the non-metamorphic units of the Tuscan Nappe, mainly represented by *Calcare Cavernoso* Fm. and cataclastic breccia (limestone and dolomitic limestone in Fig. 1b). Several orebodies, made of pyrite ± baryte ± iron oxide ± (Pb-Zn-Ag), form lensoidal bodies or small masses prevalently associated with the basement rocks, particularly close to the contact with the metadolostone of the *Grezzoni* Fm. Pyrite ores from the Baccatoio basin area contain high levels of PTE, including Tl up to about 600 mg/kg (D'Orazio et al., 2017). In addition to the Tl-bearing pyrite, a series of Tl sulfosalts occur within the orebodies, emphasizing the Tl-rich nature of these mineralizations (e.g., Biagioni et al., 2014).

The main aquifer systems of the Apuan Alps develop in the metamorphic carbonate sequence of the Apuane Unit (Doveri et al., 2013 and references therein), which is confined by impermeable phyllitic rocks of the Paleozoic basement at the bottom, and by medium to low permeability rocks (mainly shales and metasandstone) at the top. In this productive aquifer system, the low fracture development at depth enhances a strong inhomogeneity of the groundwater circulation, which is mostly affected by the well-known karst environment. Groundwater mostly flows within well-developed conduit networks, whose arrangement is guided by brittle-regime fractures, and parent faults set. Superficial fracturing, linked to unloading and physical-chemical processes, is responsible for high rates of rainfall infiltration (Doveri et al., 2019). Metamorphic dolostone, dolomitic marble, marble and cherty limestone host prominent groundwater resources mainly drained by
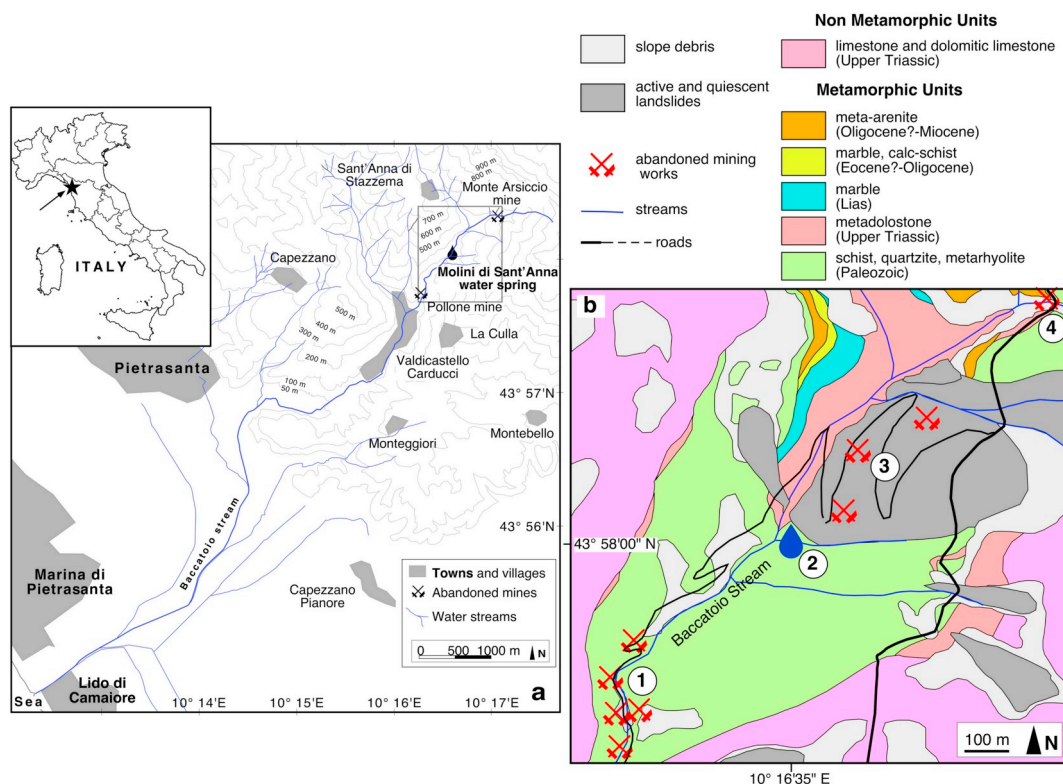
Fig. 1. a) Sketch map showing the drainage basin of the Baccatoio stream; b) geological sketch map of the area around the Molini di Sant'Anna water spring (redrawn and simplified from Conti et al., 2010). 1: Pollone mining area; 2: Molini di Sant'Anna water spring; 3: Verzalla ancient mining area; 4: Monte Arsiccio mining area.

Table 1

Minimum, maximum and average value for physico-chemical parameters and concentration of major ions in the Molini di Sant'Anna spring during the sampling period (2014–2017).

	n	Min	Max	Average	SD
T (°C)	24	11.0	11.9	11.6	0.2
pH	32	6.8	8.0	7.3	0.3
EC (µS/cm)	32	295	607	400	91
DO (mg/L)	13	7.3	10.2	9.1	0.8
HCO_3^- (mg/L)	21	156	199	182	11
Na^+ (mg/L)	21	4.6	6.9	6.4	0.5
K^+ (mg/L)	21	0.4	5.6	1.0	1.3
Ca^{2+} (mg/L)	21	54	80	66	8.2
Mg^{2+} (mg/L)	21	7.4	28.7	17.0	7.4
F^- (mg/L)	13	0.10	0.25	0.17	0.05
Cl^- (mg/L)	21	9.0	17.5	11.3	2.1
NO_3^- (mg/L)	21	0.7	4.2	1.9	0.8
SO_4^{2-} (mg/L)	21	28	149	82	40

n, number of samples; SD, standard deviation.

karst springs, whose total discharge amounts to about $5.6\,m^3/s$ (Menichini et al., 2016). Further important aquifers belong to the Tuscan Nappe and are mainly hosted in the Triassic *Calcare Cavernoso* Fm. and in the Jurassic carbonate sequence. From a hydrogeological point of view, two main aquifers are present in the upstream Baccatoio drainage basin: a) metadolostone-marble of the *Grezzoni* and *Marmi* Fms.; b) limestone-dolomitic limestone-cataclastic breccia of the *Calcare Cavernoso* Fm. The latter feeds several minor springs (outflow generally < 1 L/s), whereas the former is chiefly drained by the most important spring of the catchment area, namely the "Molini di Sant'Anna" spring (hereafter MSA; 318 m a.s.l.). This spring is located on the left hydrographic side of the Baccatoio Stream (Fig. 1), and has a yearly mean value of flow rate ≈ 40 L/s. It is an overflow spring due to the overlapping of the Paleozoic schist and quartzite rocks on the *Grezzoni* and *Marmi* Fms.

3. Sampling and methods

The MSA water was collected during different surveys from October 2014 to December 2017. Water temperature, pH, electrical conductivity (EC) and dissolved oxygen (DO) were measured on field. Alkalinity (expressed as HCO_3^-) was also determined at the sampling site by acidimetric titration with 0.1 N HCl. For laboratory analyses, water was collected in cleaned HDPE bottles and filtered through 0.45 µm nylon filters. Filtered aliquots for major cation and trace element analysis were acidified on field using ultrapure HNO_3 to pH lower than 2.0. Few water samples were collected without filtration and acidified to assess the presence of particles. Some of the water samples were analyzed for oxygen and hydrogen isotopic signature, in addition, precipitations from heavy raining events during two of the surveys were collected by runoff on hillslopes and analyzed.

Major ions were determined by ion chromatography using a Thermo ICS 900. For the anions, a Dionex IonPac AS23 analytical column was used along with the ASRS 500 suppressor. For the cations, a Dionex IonPac CS12A-5 µm analytical column was used with the CMMS 300 suppressor. Analytical precision, expressed as relative standard deviation (RSD), calculated on five replicate injections, is < 5%.

Trace elements (Li, Be, V, Cr, Mn, Fe, Co, Ni, Cu, Zn, As, Sr, Mo, Ag, Cd, Sn, Sb, Ba, Tl, Pb, Th and U) were determined using a Perkin Elmer NexION 300× ICP-MS using [103]Rh, and [209]Bi as internal standards to correct for signal fluctuations and matrix effects. Trace-element concentrations determined in a certified reference solution (IV-STOCK-1643, supplied by Inorganic Ventures), in five-repeated analyses, were used to evaluate analytical uncertainties. The accuracy was generally < 10% and the precision within 5% RSD, except for Zn (10–20% RSD). The detection limits (D.L) for each element were evaluated as the

mean value of the blank solution concentration (ten replicates) plus three times the standard deviation.

Oxygen and hydrogen stable isotopes signature was determined following the CO_2/H_2 water equilibration technique using an automatic equilibration device on line with a Finnigan Delta Plus mass spectrometer (Horita et al., 1989). The O-H isotope data are expressed by using the conventional delta notation ($\delta^{18}O$ and δD), which represents the ‰ deviation with respect to the V-SMOW standard ($\delta = [(R_{sample} / R_{standard}) - 1] \times 1000$ (‰), where R represents the $^{18}O/^{16}O$ or $D/^1H$ isotope ratio). The analytical uncertainty for $\delta^{18}O$ and δD was ± 0.05‰ and ± 0.7‰, respectively.

Hourly monitoring of temperature and EC was also performed at the MSA spring by using a CTD diver (Eijkelkamp Soil & Water) data logger from March 25, 2015 to November 5, 2015. Furthermore, several measures of the spring flow rate (Q [m^3/s]) were obtained in the period December 2015–December 2016 using a "Cipolletti" weir and applying the standard equation $Q = 1.86\,L(h)^{3/2}$, where L [m] is the weir length and h [m] is the water level.

Geochemical modeling was investigated using PHREEQC software (Parkhurst and Appelo, 1999).

4. Results

The physico-chemical parameters and major-element data in water collected during the different surveys are reported in Table 1. Water temperature ranged between 11.0 °C and 11.9 °C, a relatively narrow range compared with average air temperature in the area upstream of the spring (in the range 10–15 °C), indicating a negligible influence of the atmospheric temperature variations on the groundwater body drained by the MSA spring. The pH value ranged from 6.8 to 8.0. Dissolved oxygen was in the range 7.3–10.2 mg/L, suggesting that infiltrating waters, saturated with atmospheric oxygen, undergo reactions removing oxygen along the groundwater flow paths. The EC range was from 295 to 607 µS/cm, significantly higher than the range 250–300 µS/cm of most Apuan Alps springs fed by similar aquifers (metadolostone and marble) (Doveri et al., 2013, 2019). The flow rate ranged from about 10 L/s, during the dry period, to about 100 L/s, in the wet period. Discharge peaks of the order of 200 L/s also occurred after heavy rainstorms. Such behavior is congruent with the typical high variability of karst springs and points out the strong linkage between rainfall and spring flow rate. The EC measured by the CTD diver recorded a sharp decrease from 590 to 380 µS/cm coupled with the increase of the spring flow rate, as a fast response (hours) to heavy rainfall events, followed by a relatively long-lasting lag to restoration of the pristine EC conditions (days).

The ionic dominance pattern of the water samples for major cations and anions is $Ca^{2+} > Mg^{2+} > Na^+ > K^+$ and $HCO_3^- > SO_4^{2-} > Cl^- > NO_3^- > F^-$ (Table 1). All water samples fall within the Italian guideline levels for major constituents for drinking water. According to the Piper diagram (Fig. 2), the MSA waters range from the Ca-HCO3 to the Ca(Mg)-HCO3(SO4) facies. The plot clearly shows that the MSA samples lie on straight lines in the diagram, suggesting a two-component mixing.

Trace-element data are presented in Table 2. The concentration of trace elements in MSA water is below the thresholds imposed by EU and Italian Regulations for groundwater except for Mn and Tl. It is worth to note that the PTE usually associated to Tl in the mineralizations located within the Baccatoio drainage basin (D'Orazio et al., 2017), namely Fe, Mn, As, Sb, Pb, Zn, Cu, Cd, Pb, Ag, are dissolved in the MSA water at low to very low concentration levels (Table 2).

Manganese concentrations are highly variable ranging between 0.25 and 118 µg/L (average: 40 ± 37 µg/L), exceeding the 50 µg/L regulatory limit for groundwater in many samples. Thallium concentrations are invariably higher than the 2 µg/L maximum allowable limit for groundwater, ranging from 4.3 to 27.8 µg/L (average: 13.3 ± 7.1 µg/L). The Tl concentration in the spring water appears to
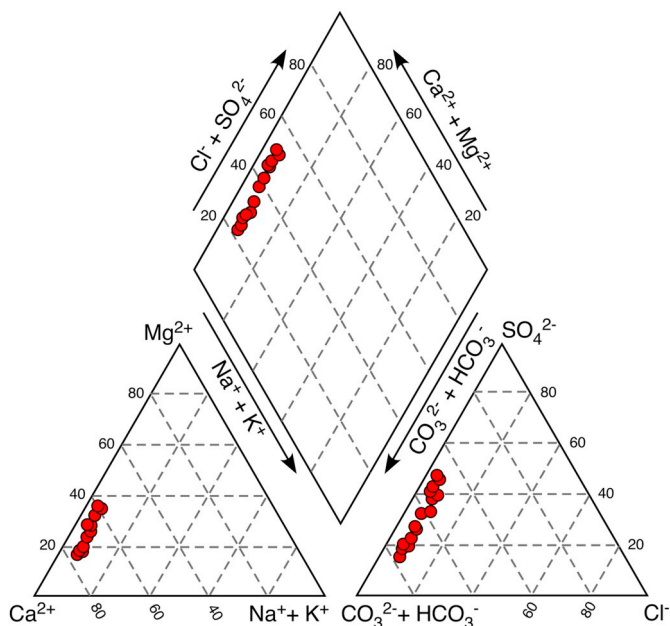
Fig. 2. Piper diagram for the MSA waters.

be roughly related to the amount of precipitations (Fig. 3), and inversely correlated with the spring discharge (Fig. 4). In particular, we observe that periods of low rainfall are correlated with trends of increasing Tl concentrations, whereas the opposite occurs during high rainfall periods (Fig. 3). Rainfall and changes in Tl concentrations are not strictly synchronous, suggesting a delay between recharge of the system and changes in Tl concentrations.

Chemical data show that Tl is positively correlated with Sr and SO_4^{2-} (Fig. 5).

Systematic differences between filtered and unfiltered samples are observed for Fe, and to a lesser extent for Mn, showing higher concentration in the unfiltered waters (Table 2) and likely reflecting the occurrence of Fe-(Mn)-bearing particles that do not pass through the 0.45 μm filter pores. No significant variations in Tl concentration between filtered and unfiltered samples are observed.

The O and H isotope data on MSA water overlaps the Apuan Alps meteoric water line reported by Mussi et al. (1998), or are slightly displaced (Fig. 6), indicating a meteoric origin. Despite sampling was performed in different hydrologic periods under high and low flow rates, the isotopic signature of the MSA water varied within a relatively small range (from −6.72 to −6.37‰ and from −40.4‰ to −37.0 for $\delta^{18}O$ and δD, respectively, Table 3). This is in contrast to the typical isotopic variability of most Apuan Alps karst springs (Doveri et al., 2013, 2019), which reflect the seasonal isotopic variability of rainfall (e.g., about ± 2.5‰ for $\delta^{18}O$). The deuterium excess (d = δD − $8\delta^{18}O$, Dansgaard, 1964) of the MSA spring ranges from 12.2 to 16.5, in agreement with the rainfall of the Apuan Alps area (Mussi et al., 1998).

5. Discussion

As already stated, the composition of water from the MSA spring plots along straight lines in each of fields of the Piper diagram (Fig. 2), suggesting the occurrence of mixing between two end-members. One end-member is represented by a Ca-HCO₃ water-type, which indicates Ca-carbonates as main host rocks. The other end-member is relatively enriched in sulfate. The positive correlation between SO_4^{2-} and Tl (Fig. 5b), indicates that the sulfate-rich end-member is the Tl-contaminated one. The Ca^{2+}/Mg^{2+} molar ratio vs. SO_4^{2-} diagram (Fig. 7) defines a hyperbolic trend in agreement with the two-component mixing hypothesis (Langmuir et al., 1978).

In the studied area, Tl is contained in primary sulfides (mainly pyrite) and sulfosalts, in secondary minerals such as Fe-Mg-Al-K sulfates and Fe-oxyhydroxides (D'Orazio et al., 2017). Sulfates and Fe-oxyhydroxides derive from pyrite oxidation. Upslope the MSA spring outflow these materials occur diffusely mainly along the left orographic side of the Baccatoio Stream (Fig. 1). In the area, pyrite undergoes oxidation in contact with oxygen and water producing a solution containing acidity and heavy metals (namely acid drainage), including thallium (Perotti et al., 2017). It is therefore conceivable that the sulfate-rich and Tl-contaminated end-member forms by interaction of water with the above-mentioned Tl-bearing materials.

However, this process should generate water with high concentrations of other PTE (especially Fe, Mn, As, Sb) in addition to Tl and SO_4^{2-}. Since the MSA spring produces water with high and variable Tl and sulfate concentrations, but low to very low levels of Fe and the other PTE, we can hypothesize that the contaminated end-member, before reaching the MSA spring, loses dissolved metals as a result of interactions with aquifer rocks.

5.1. Hydrogeochemical modeling

The hypothesis of binary mixing was better constrained by using PHREEQC (Parkhurst and Appelo, 1999). The modeling indicates that a simple mixing between a Ca-HCO₃ water and a sulfate-rich acid drainage cannot account for the pH values of MSA water and for the observed Ca^{2+}/Mg^{2+} vs. SO_4^{2-} geochemical pattern (Fig. 7). The observation data can be better predicted by a two-stage process where the sulfate- and thallium-rich acid drainage first interacts with dolostones of the *Grezzoni* Fm. dissolving dolomite until circum-neutral pH, and then mixes with a Ca-HCO₃ water.

In particular, to model the data, the geochemical parameters typical of an acid drainage of the area (e.g. Mt. Arsiccio mine site; Perotti et al., 2017) were used [T = 11 °C; pH = 2.2; Ca^{2+} = 320 mg/L; Mg^{2+} = 150 mg/L; SO_4^{2-} = 6500 mg/L; Sr 1.80 mg/L]. During the first stage of the process about 0.03 mol/L of dolomite dissolves, due to the interaction of acidic water with dolostones, and saturation with gypsum and schwertmannite occurs as increasing pH (Bigham et al., 1996; Yu et al., 1999). The water so formed has a pH of 6.6, a Ca^{2+}/Mg^{2+} molar ratio of about 1.0 (close to what expected for dolomite), SO_4^{2-} and Sr content of about 3100 and 1.75 mg/L, respectively, and it represents the sulfate-rich contaminated end-member. This term mixes in different proportion with a Ca-HCO₃ water that must have a composition in the order of Ca^{2+} = 70 mg/L; Mg^{2+} = 6 mg/L; SO_4^{2-} = 16 mg/L; Sr 0.08 mg/L and T = 12 °C, pH = 7.8. These values are consistent with the calcium-bicarbonate waters outflowing in the basin. Calculation indicates variable undersaturation with calcite (calcite SI from −0.7 to −0.3) during mixing and that the mixing proportions of the contaminated end-member range from about 3% to 0.3%. The results of the second stage of the model are graphically shown in Fig. 7.

The Sr concentration calculated by the model (in the range between 136 and 82 μg/L) mimics what actually measured at MSA (see Table 2 and Fig. 5a). Thallium species and related reactions were not included in PHREEQC. However, starting from a Tl content in the acidic drainage of about 950 μg/L (a value consistent with Mt. Arsiccio outflows (Perotti et al., 2017)), a simple mass-balance approach fits quite well the Tl concentration of MSA water (data not shown). Some discrepancy between the experimental and calculated values occurs at the lowest Tl concentration (4.3 and 2.8 μg/L, respectively). This may partly reflect a non-conservative behavior of thallium during mixing, and requires further investigations. Actually Mn-oxides are effective in sorbing heavy metals cations under a wide range of pH conditions due to their low point of zero charge (Davis and Kent, 1990), including thallium (Wan et al., 2014).

The model also suggests that the PTEs that characterize acid drainages were scavenged during the neutralization of the acidic plume by

Table 2
Trace-element concentrations (μg/L) of water samples from the Molini di Sant'Anna spring.

Date (dd-mm-yy)	Li	V	Cr	Mn	Fe	Co	Ni	Cu	Zn	As	Sr	Mo	Ag	Cd	Sn	Sb	Ba	Tl	Pb	Th	U
D.L. (μg/L)	0.07	0.04	0.2	0.2	6	0.01	0.4	3	15	0.04	0.5	0.2	0.02	0.04	0.05	0.05	0.7	0.05	0.2	0.01	0.01
12-10-14[a]	0.95	< D.L.	< D.L.	87	1337	0.52	7.4	< D.L.	< D.L.	0.55	118	< D.L.	< D.L.	0.14	–	0.35	61	17.3	< D.L.	< D.L.	0.46
02-12-14	0.40	< D.L.	< D.L.	12.7	14	0.15	3.4	< D.L.	< D.L.	0.60	84	0.22	< D.L.	0.06	–	0.41	55	4.3	< D.L.	< D.L.	0.32
03-12-14	0.48	< D.L.	< D.L.	22.0	13	0.18	3.8	< D.L.	< D.L.	0.14	89	0.26	< D.L.	0.05	–	0.40	48	5.4	< D.L.	< D.L.	0.35
09-12-14	0.58	< D.L.	< D.L.	46	11	0.20	5.1	< D.L.	28	0.26	96	0.74	< D.L.	0.04	–	0.41	47	8.0	< D.L.	< D.L.	0.39
25-02-15	0.50	< D.L.	< D.L.	< D.L.	11	0.09	4.4	< D.L.	< D.L.	0.13	87	0.40	< D.L.	< D.L.	–	0.37	47	10.2	< D.L.	< D.L.	0.24
25-02-15[a]	0.50	0.07	< D.L.	4.5	976	0.13	4.8	< D.L.	< D.L.	0.69	87	0.29	< D.L.	0.09	–	0.38	66	9.4	< D.L.	0.02	0.37
28-04-15	0.90	0.04	< D.L.	104	106	0.62	8.1	< D.L.	< D.L.	0.37	104	0.24	< D.L.	0.14	< D.L.	0.42	58	14.1	0.3	< D.L.	0.40
27-06-15	1.05	< D.L.	< D.L.	1.8	25	0.11	6.5	< D.L.	< D.L.	0.04	120	< D.L.	< D.L.	0.05	< D.L.	0.31	41	19.0	< D.L.	< D.L.	0.51
15-09-15	1.21	< D.L.	< D.L.	118	83	0.71	10.2	6	21	0.21	127	< D.L.	< D.L.	0.15	–	0.46	56	26.2	0.6	0.03	0.44
30-09-15	1.36	< D.L.	< D.L.	95	27	0.49	10.1	< D.L.	< D.L.	0.07	135	< D.L.	0.14	0.11	< D.L.	0.29	55	27.8	< D.L.	< D.L. < 0.01	0.53
30-09-15[a]	1.27	< D.L.	< D.L.	105	1154	0.41	10.9	< D.L.	20	0.47	133	< D.L.	0.23	0.27	< D.L.	0.29	55	24.1	< D.L.	0.03	0.44
08-10-15	1.33	< D.L.	< D.L.	< D.L.	27	0.12	4.5	< D.L.	< D.L.	< D.L.	140	0.29	< D.L.	< D.L.	< D.L.	0.27	58	24.5	< D.L.	< D.L.	0.42
05-11-15	0.76	< D.L.	< D.L.	0.2	23	0.12	4.8	< D.L.	< D.L.	0.13	109	< D.L.	< D.L.	< D.L.	0.07	0.43	56	20.0	< D.L.	< D.L.	0.47
30-12-15	0.99	< D.L.	< D.L.	52	45	0.38	7.7	< D.L.	< D.L.	0.14	124	< D.L.	< D.L.	0.09	< D.L.	0.30	55	18.6	1.7	< D.L.	0.28
05-01-16	0.40	< D.L.	< D.L.	16.8	27	0.15	4.0	< D.L.	< D.L.	0.15	95	0.22	< D.L.	0.06	< D.L.	0.32	43	15.8	< D.L.	< D.L.	0.28
05-01-16R	0.42	< D.L.	< D.L.	14.3	22	0.15	3.8	< D.L.	< D.L.	0.25	95	0.24	< D.L.	0.06	< D.L.	0.38	52	15.1	< D.L.	< D.L.	0.28
11-01-16	0.34	< D.L.	< D.L.	5.7	26	0.12	3.3	< D.L.	< D.L.	0.32	87	< D.L.	< D.L.	0.04	< D.L.	0.33	45	8.3	< D.L.	< D.L.	0.24
13-01-16	0.39	0.04	< D.L.	21.4	22	0.22	3.9	< D.L.	< D.L.	0.21	95	0.30	< D.L.	0.05	< D.L.	0.43	55	10.2	< D.L.	< D.L.	0.33
26-01-16	0.74	0.12	3.3	51	133	0.44	6.5	< D.L.	120	0.35	102	0.30	< D.L.	0.07	0.24	0.39	50	12.5	< D.L.	< D.L.	0.35
06-02-16	0.47	0.11	< D.L.	16.3	13	0.18	4.4	< D.L.	< D.L.	0.27	91	0.30	< D.L.	< D.L.	< D.L.	0.44	49	7.8	< D.L.	0.07	0.36
07-02-16	0.49	< D.L.	< D.L.	21.3	21	0.20	4.6	< D.L.	< D.L.	0.27	90	0.21	< D.L.	< D.L.	0.30	0.37	48	8.1	< D.L.	0.04	0.39
08-02-16	0.35	< D.L.	< D.L.	0.9	19	0.09	3.5	< D.L.	< D.L.	0.08	82	< D.L.	< D.L.	< D.L.	0.37	0.37	43	7.6	< D.L.	< D.L.	0.21
09-02-16	0.32	0.13	< D.L.	1.8	15	0.10	3.4	< D.L.	< D.L.	0.32	82	< D.L.	< D.L.	< D.L.	< D.L.	0.33	41	4.9	< D.L.	< D.L.	0.25
10-02-16	0.31	< D.L.	< D.L.	2.9	28	0.10	3.4	< D.L.	< D.L.	0.26	77	0.22	< D.L.	< D.L.	< D.L.	0.31	45	4.4	< D.L.	< D.L.	0.20
11-02-16	0.34	0.09	< D.L.	5.4	20	0.11	3.6	< D.L.	17	0.56	83	0.23	< D.L.	0.05	< D.L.	0.35	49	4.3	0.81	< D.L.	0.27
12-02-16	0.39	< D.L.	< D.L.	14.0	33	0.15	4.7	< D.L.	< D.L.	0.64	86	0.30	< D.L.	< D.L.	< D.L.	0.39	56	5.3	< D.L.	< D.L.	0.32
22-03-16	0.68	< D.L.	< D.L.	74	23	0.45	5.8	< D.L.	< D.L.	0.24	93	0.25	< D.L.	0.09	< D.L.	0.40	55	8.9	< D.L.	< D.L.	0.34
06-04-16	0.71	< D.L.	< D.L.	71	26	0.46	6.4	< D.L.	< D.L.	0.22	96	0.21	< D.L.	0.09	< D.L.	0.40	56	11.7	< D.L.	< D.L.	0.35
14-09-16	1.09	< D.L.	< D.L.	34	44	0.22	7.7	< D.L.	< D.L.	< D.L.	121	0.25	< D.L.	0.10	< D.L.	0.29	56	20.2	< D.L.	< D.L.	0.41
19-12-16	0.86	< D.L.	< D.L.	59	39	0.37	6.3	< D.L.	< D.L.	0.13	110	0.26	< D.L.	0.08	< D.L.	0.40	56	15.0	0.24	< D.L.	0.37
08-02-17	0.49	< D.L.	< D.L.	14.0	57	0.16	3.9	6	< D.L.	0.53	84	< D.L.	< D.L.	0.25	< D.L.	0.38	47	6.6	0.30	< D.L.	0.34
01-09-17	1.29	< D.L.	< D.L.	80	76	0.50	8.4	< D.L.	< D.L.	0.07	122	0.29	< D.L.	< D.L.	0.11	0.23	54	22.1	< D.L.	0.01	0.41
07-12-17	1.03	< D.L.	< D.L.	84	39	0.50	8.8	< D.L.	< D.L.	0.10	127	0.29	< D.L.	< D.L.	0.12	0.29	52	20.9	< D.L.	< D.L.	0.40

D.L., detection limit; R, replicate analysis; −, not detected. The concentrations of Be, B and Se were always found below the D.L. of 0.01, 20 and 1 μg/L, respectively.
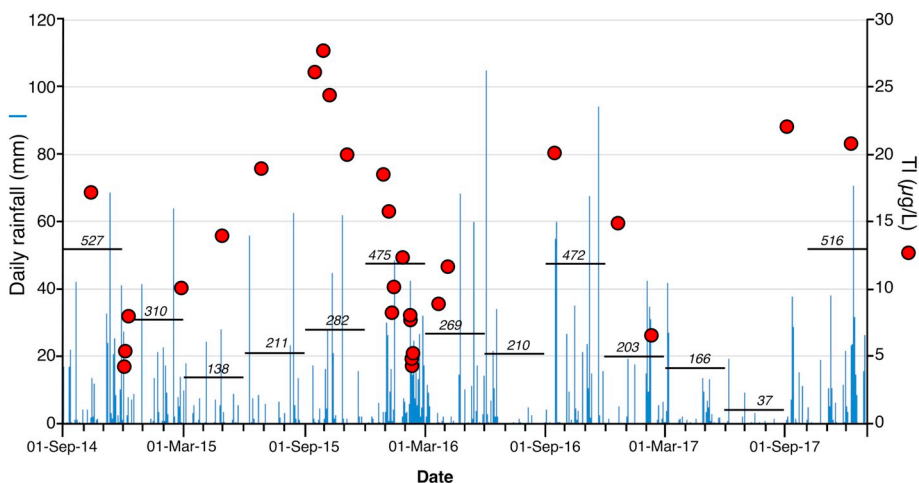
[a] Unfiltered sample

Fig. 3. Comparison between daily rainfall at the Pietrasanta raingauge (www.sir.toscana.it) and Tl concentrations in water from the MSA spring. The numbers in italics are the cumulative rainfall (mm) over the indicated time intervals (black horizontal segments).
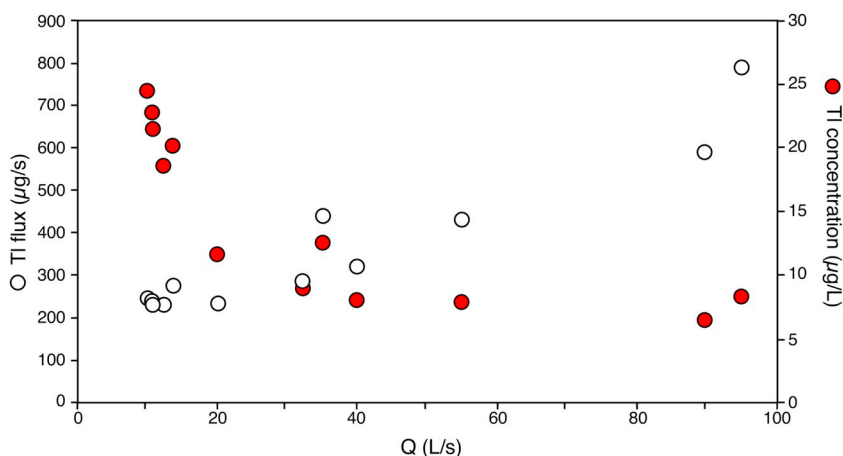

Fig. 4. Plot of Tl concentration (red circles) and Tl flux (empty circles) at MSA spring as a function of the spring flow rate (Q). (For interpretation of the references to color in this figure legend, the reader is referred to the web version of this article.)

carbonate minerals. In particular, after carbonate interaction the water has a strong supersaturation with hydrous ferric oxides such as goethite (SI: 9.8) and amorphous $Fe(OH)_3$ (SI: 4.4) and Mn-oxides (birnessite, SI: 7.7) allowing the nucleation and growth of particles and the removal of iron and manganese. The Fe and Mn precipitates that form affect the fate of some potentially toxic elements. In particular, arsenic and lead

are readily sorbed onto iron oxyhydroxides even at circumneutral pH (Bowell, 1994; Webster et al., 1998). Adsorption calculations onto hydrous ferric oxide with PHREEQC using the two-layer model by Dzombak and Morel (Dzombak and Morel, 1990) for surface complexation reactions on both weak and strong sites indicate that about 98.4 wt% of the original $As(OH)_4^-$ is adsorbed onto hydrous ferric
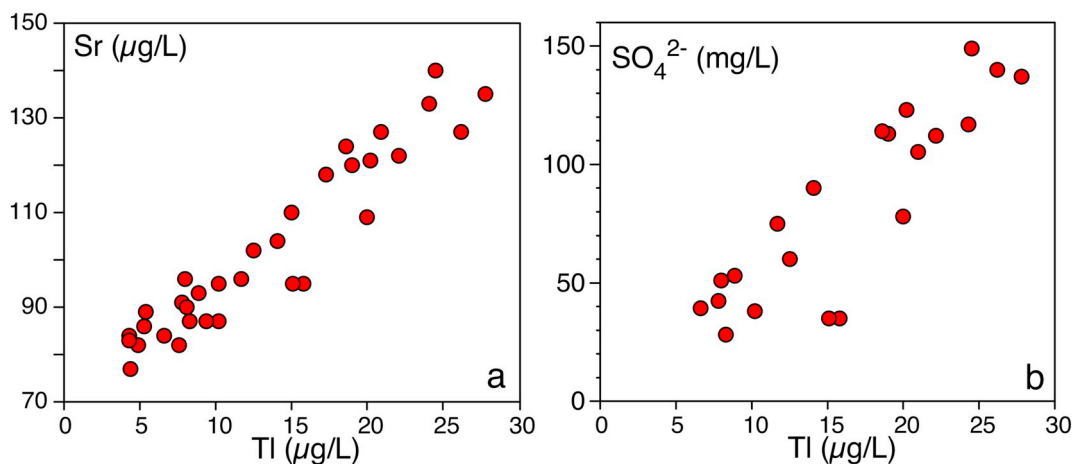

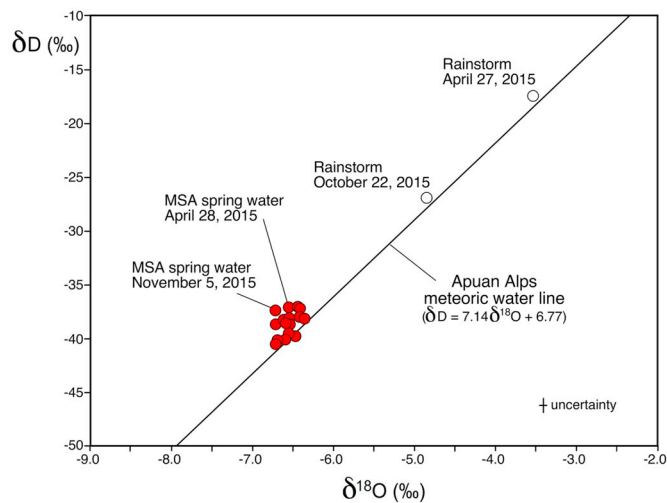**Fig. 5.** Plot of Sr vs. Tl (a), and SO_4^{2-} vs. Tl (b) in the MSA spring water.

Fig. 6. Plot of δD (‰) vs. δ^{18}O (‰) for water samples from the Molini di Sant'Anna spring. The rainwater of rainstorm events of April 27 and October 22, 2015 are also plotted. The Apuan Alps meteoric water line determined by Mussi et al. (1998) is drawn for comparison.

Table 3

Oxygen and hydrogen isotope ratios of the Molini di Sant'Anna spring water (2014–2016). The O-H isotopic data are expressed by using the conventional delta notation (δ^{18}O and δD), which represents the ‰ deviation with respect to the V-SMOW standard (δ = [(Rsample/Rstandard) − 1] ∗ 1000 (‰) where R represents the ^{18}O/^{16}O or D/H isotopic ratio).

Date dd/mm/yyyy	δ^{18}O (‰)	δD (‰)
27-10-14	−6.45	−37.0
03-12-14	−6.72	−38.6
09-12-14	−6.69	−40.1
28-04-15	−6.56	−37.0
30-09-15	−6.56	−38.0
08-10-15	−6.37	−38.0
16-10-15	−6.41	−37.1
05-11-15	−6.72	−37.3
30-12-15	−6.59	−38.5
05-01-16	−6.56	−39.4
11-01-16	−6.55	−38.6
26-01-16	−6.60	−40.0
06-02-16	−6.43	−37.9
22-03-16	−6.62	−38.2
06-04-16	−6.48	−39.7
14-09-16	−6.72	−40.4

oxide, buffering the As concentration in fluid with respect to acid drainage to about 0.15 μg/L. This value is close to the average As concentration of 0.2 μg/L actually measured in MSA waters. The slightly higher As concentration in unfiltered samples compared to filtered ones (Table 2), supports the hypothesis that As occurs in the particulate fraction of the spring water.

5.2. Groundwater flow conceptual model

As reported in the Results section, the MSA oxygen and hydrogen isotopic signature varied within a relatively small range, despite sampling was performed in different hydrological regimes and during different seasons. Hence, the two mixing end-members contributing to the total flux at MSA have a very similar isotope signature and/or one of them enter in the mixing with very low percentage, which is unable to lead to significant isotopic variations.

The negligible variation of the O-H isotopic signature also suggests the aquifer feeding MSA promotes a homogenization of waters infiltrated during a period of one or more years and seems to preserve the
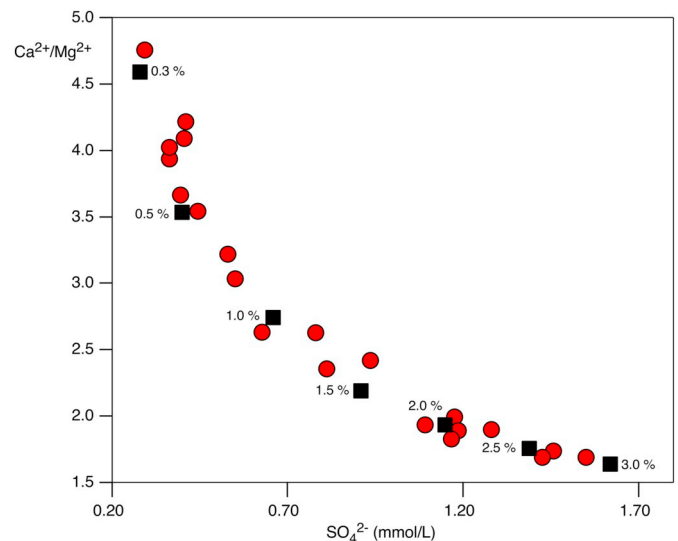

Fig. 7. Plot of Ca^{2+}/Mg^{2+} molar ratio as a function of SO$_4^{2-}$ concentration in the MSA water (red circles). The black squares represent calculated values obtained for a two-component mixing, where a Ca-HCO$_3$-type water (Ca^{2+}/Mg^{2+} molar ratio = 7.1, SO$_4^{2-}$ = 0.17 mmol/L and pH = 7.8) mixes with a sulfate-rich, thallium contaminated end member (Ca^{2+}/Mg^{2+} molar ratio = 1.0, SO$_4^{2-}$ = 32.3 mol/L and pH = 6.6) (see Section 5.1 for explanations). Numbers refer to the mixing percentage of SO$_4^{2-}$ and Tl contaminated end member. (For interpretation of the references to color in this figure legend, the reader is referred to the web version of this article.)

spring from the short-term input of rainfall water in significant quantity. This seems to be confirmed by data collected during the April and October 2015 heavy rainfall events, characterized by a very heavier isotope signature (from −3.54 to −4.85‰ and from −17.4 to −26.9‰ for δ^{18}O and δD, respectively) with respect to the typical isotopic values of MSA (on average − 6.5‰ and −39‰ for δ^{18}O and δD, respectively). This indicates that, despite the fast increase in the MSA flow rate during these showers, the infiltrating rainwater did not directly supply the spring outflow. This behavior could be reasonably due to the so called piston flow effect: the hydraulic pressure propagation, due to heavy rainfall infiltration, causes a displacement (without mixing) of groundwater stored in the aquifer towards the spring, yielding an increase in spring outflow with respect to the normal underground flow.

The diagram of Fig. 4 shows that the concentration of Tl in the MSA spring water decreases as the spring flow rate (Q$_{tot}$) increases. On the contrary, the Tl mass discharge rate (obtained multiplying the Tl concentration by Q$_{tot}$) has a rough positive correlation with Q$_{tot}$. Such behavior necessarily requires an increase of Q for both the components involved in the mixing and that the rise of Q is higher for the Ca-HCO$_3$ component than for the Tl-enriched one. Therefore the piston flow mechanism acts with different magnitude on both the components, thus affecting the proportion of mixing components at the MSA spring. However, the simple binary mixing hypothesis obtained by geochemical modeling implies that the contaminated end-member has nearly constant composition, suggesting that, at least in the surveyed time, the changes in hydrologic boundary conditions do not significantly affect the interaction process of acidic waters and dolomitic rocks.

The achieved information enables a hydrogeological model to be formulated (Fig. 8). In the model, the contaminated water originates along the left orographic side of the Baccatoio Stream, where Tl-bearing minerals are mainly diffused, and it reaches the MSA aquifer. Owing to the occurrence of a favorable fracture network and/or to the higher density of contaminated water with respect to freshwater, the former mainly flows towards the lower part of the saturated zone, close to the contact with the impervious substratum (schist, quartzite and
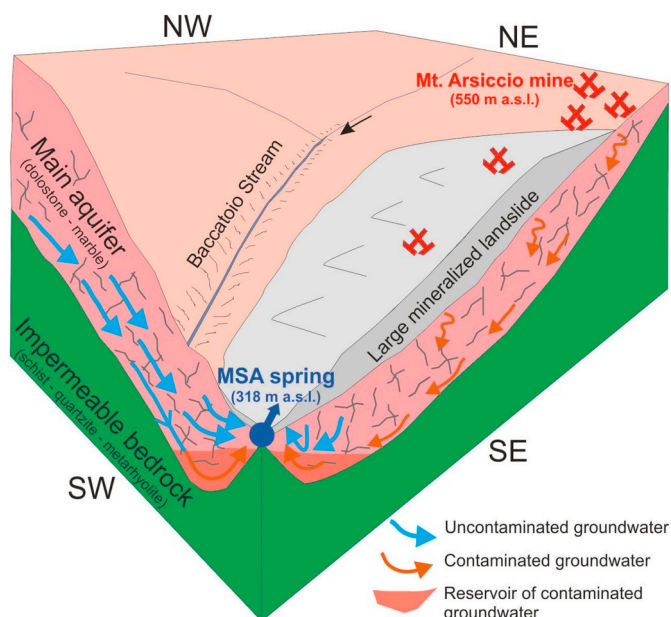
Fig. 8. Schematic hydrogeological model of the Molini di Sant'Anna (MSA) spring; a.s.l., above sea level.

metarhyolite). Due to the structural setting that makes the MSA an overflow spring, the contaminated water forms a reservoir in the sector of the aquifer that close to the spring zone dips beneath the impermeable rocks. Given the typical hydrodynamic behavior of this kind of outflow context, an uprise of groundwater from the contaminated reservoir may occur. This uprising water interacts before reaching the MSA spring with the Ca-HCO$_3$ water flowing into the shallower and more transmissive part of the aquifer.

6. Conclusions

The past-mining area nearby the Valdicastello Carducci village, in the Tuscan Region of Italy, is characterized by thallium-bearing orebodies. In this setting, a Tl-contaminated spring was used as drinking water supply. The Tl-contamination in the spring results from the binary mixing at different scale of two sources. The uncontaminated component is constituted by Ca-HCO$_3$-type water that mixes with waters from a contaminated body which formed by the interaction of acid drainages generated by the weathering of Tl-hosting mineral phases with dolostone rocks.

This process yield acidic neutralization and the scavenging of most of the potentially toxic elements released during weathering mostly due to adsorption onto the iron and manganese oxyhydroxides that formed during pH changes. During this process, thallium behaves almost conservatively and correlates with sulfate and strontium in the spring waters. Geochemical and isotopic data and hydrogeological constraints reveal that a near steady-state hydrological regime is attained, possibly driven by precipitations through piston-flow water displacements.

On this ground, additional studies are necessary for the development of strategies and treatments allowing thallium contamination to be mitigated and to manage this water resource.

Furthermore, this study highlights that a policy to ensure safe water for human consumption must account for the interaction between environmental threats and human heal.

References

Baoxiang, Z., Fanhai, M., 2011. Delineation methods and application of groundwater source protection zone. In: Water Resource and Environmental Protection (ISWREP), 2011 International Symposium on Volume: 1 (IEEE Conference Publications). pp. 66–69.

Biagioni, C., D'Orazio, M., Vezzoni, S., Dini, A., Orlandi, P., 2013. Mobilization of Tl-Hg-As-Sb-(Ag,Cu)-Pb sulfosalt melts during low-grade metamorphism in the Alpi Apuane (Tuscany, Italy). Geology 41, 747–750.

Biagioni, C., Bonaccorsi, E., Moëlo, Y., Orlandi, P., Bindi, L., D'Orazio, M., Vezzoni, S., 2014. Mercury-arsenic sulfosalts from Apuan Alps (Tuscany, Italy). III. Arsiccioite, AgHg2TlAs2S6, a new mineral from the Monte Arsiccio mine: occurrence, crystal structure, and crystal chemistry of the routhierite isotypic series. Mineral. Mag. 78 (1), 101–117.

Biagioni, C., D'Orazio, M., Lepore, G.O., D'Acapito, F., Vezzoni, S., 2017. Thallium-rich rust scales in drinkable water distribution systems: a case study from northern Tuscany, Italy. Sci. Total Environ. 587-588, 491–501.

Bigham, J.M., Schwertmann, U., Traina, S.J., Winland, R.L., 1996. Schwertmannite and the chemical modeling of iron in acid sulfate waters. Geochim. Cosmochim. Acta (12), 2111–2121.

Bowell, R.J., 1994. Sorption of arsenic by iron oxides and oxyhydroxides in soils. Appl. Geochem. 9 (3), 279–286.

Campanella, B., Onor, M., D'Ulivo, A., Giannecchini, R., D'Orazio, M., Petrini, R., Bramanti, E., 2016. Human exposure to thallium through tap water: a study from Valdicastello Carducci and Pietrasanta (northern Tuscany, Italy). Sci. Total Environ. 548–549, 33–42.

Campanella, B., Casiot, C., Onor, M., Perotti, M., Petrini, R., Bramanti, E., 2017. Thallium release from acid mine drainages: speciation in river and tap water from Valdicastello mining district (northwest Tuscany). Talanta 171, 255–261.

Carmignani, L., Kligfield, R., 1990. Crustal extension in the Northern Apennines: the transition from compression to ex-tension in the Alpi Apuane Core Complex. Tectonics 9 (6), 1275–1303.

Casiot, C., Egal, M., Bruneel, O., Verma, N., Parmentier, M., Elbaz-Poulichet, F., 2011. Predominance of aqueous Tl(I) species in the river system downstream from the abandoned Carnoules Mine (southern France). Environ. Sci. Technol. 45 (6), 2056–2064.

Chowdhury, S., Jafar Mazumder, M.A., Al-Attas, O., Husain, T., 2016. Heavy metals in drinking water: occurrences, implications and future needs in developing countries. Sci. Total Environ. 569–570, 476–488.

Cidu, R., Biddau, R., Fanfani, L., 2009. Impact of past mining activity on the quality of groundwater in SW Sardinia (Italy). J. Geochem. Explor. 100, 125–132.

Colombaioni, L., Onor, M., Benedetti, E., Bramanti, E., 2017. Thallium stimulates ethanol production in immortalized hippocampal neurons. PLoS ONE 12 (11), e0188351.

Conti, P., Di Pisa, A., Gattiglio, M., Meccheri, M., 1993. Prealpine basement in the Alpi Apuane (Northern Apennines, Italy). In: Von Raumer, J.F., Neubauer, F. (Eds.), Pre-Mesozoic Geology in the Alps. Springer Verlag, pp. 609–621.

Conti, P., Massa, G., Meccheri, M., Carmignani, L., 2010. Geological map of the Stazzema area (Alpi Apuane, Northern Apennines, Italy). Scale 1/10000. Centro di Geotecnologie, Università di Siena.

Dansgaard, W., 1964. Stable isotopes in precipitation. Tellus 16, 436–468.

Davis, J.A., Kent, D.B., 1990. Surface complexation modeling in aqueous geochemistry. Rev. Mineral. 23, 177–260.

D'Orazio, M., Biagioni, C., Dini, A., Vezzoni, S., 2017. Thallium-rich pyrite ores from the Apuan Alps, Tuscany, Italy: constraints for their origin and environmental concern. Miner. Deposita 52, 687–707.

Doveri, M., Menichini, M., Cerrina Feroni, A., 2013. Stable water isotopes as fundamental tool in karst aquifer studies: some results from isotopic applications in the Apuan Alps carbonatic complexes (NW Tuscany). Italian J. Eng. Geol. Environ. 1, 33–50.

Doveri, M., Piccini, L., Menichini, M., 2019. Hydrodynamic and Geochemical Features of Metamorphic Carbonate Aquifers and Implications for Water Management: The Apuan Alps (NW Tuscany, Italy) Case Study. In: Younos, T., Schreiber, M., Kosič Ficco, K. (Eds.), Karst Water Environment. The Handbook of Environmental Chemistry 68 Springer Cham.

Dzombak, D.A., Morel, F.M.M., 1990. Surface Complexation Modeling: Hydrous Ferric Oxide. Wiley and Sons, NY.

Horita, J., Ueda, A., Mizukami, K., Takatori, I., 1989. Automatic δD and δ18O analyses of multi-water samples using H2– and CO2–water equilibration methods with a common equilibration set-up. Appl. Radiat. Isot. 40, 801–805.

Jamleson, H.E., 2011. Geochemistry and mineralogy of solid mine waste: essential knowledge for predicting environmental impact. Elements 7 (6), 380–386.

Langmuir, C.H., Vockejr, R.D., Hanson, G.N., Hart, S.R., 1978. A general mixing equation with applications to Icelandic basalts. Earth Planet. Sci. Lett. 37, 380–392.

Martınez Navarrete, C., Grima Olmedo, J., Duran Valsero, J.J., Gomez, J.D., Luque Espinar, J.A., de la Orden, G.J.A., 2008. Groundwater protection in Mediterranean countries after the European water framework directive. Environ. Geol. 54, 537–549.

Menichini, M., Doveri, M., Piccini, L., 2016. Hydrogeological and geochemical overview of the karst aquifers in the Apuan Alps (Northwestern Tuscany, Italy). Ital. J. Groundw. AS16–198, 15–23.

Molli, G., Meccheri, M., 2012. Structural inheritance and style of reactivation at mid-crustal levels: a case study from the Alpi Apuane (Tuscany, Italy). Tectonophysics 579, 74–87.

Mussi, M., Leone, G., Nardi, I., 1998. Isotopic geochemistry of natural waters from the Alpi Apuane-Garfagnana area, Northern Tuscany, Italy. Mineral. Petrogr. Acta XLI, 163–178.

Nordstrom, D.K., 2011. Hydrogeochemical processes governing the origin, transport and fate of major and trace elements from mine wastes and mineralized rocks to surface waters. Appl. Geochem. 26, 1777–1791.

Parkhurst, D.L., Appelo, C.A.J., 1999. User's guide to PHREEQC a computer program for speciation, batch-reaction, one-dimensional transport, and inverse geochemical calculations. U.S. Geol. Surv. Water. Resour. Inv. Rep. 99–4259 (312 pp, version 2.15.07).

Perotti, M., Petrini, R., D'Orazio, M., Ghezzi, L., Giannecchini, R., Vezzoni, S., 2017.

Thallium and other potentially toxic elements in the Baccatoio Stream Catchment (Northern Tuscany, Italy) receiving drainages from abandoned mines. Mine Water Environ. https://doi.org/10.1007/s10230-017-0485-x.

Peter, J.A.L., Viraraghavan, T., 2005. Thallium: a review of public health and environmental concerns. Environ. Int. 31, 493–501.

Petrini, R., Cidu, R., Slejko, F.F., 2016. Thallium Contamination in the Raibl Mine Site Stream Drainage System (Eastern Alps, Italy). Mine Water Environ. 35, 55–63.

Rickwood, C.J., King, M., Huntsman-Mapila, S., 2015. Assessing the fate and toxicity of thallium I and thallium III to three aquatic organisms. Ecotoxicol. Environ. Saf. 115, 300–308.

Siegel, F.R., 2002. Environmental Geochemistry of Potentially Toxic Metals. Springer, Berlin.

Tchounwou, P.B., Yedjou, C.G., Patlolla, A.K., Sutton, D.J., 2012. Heavy metal toxicity and the environment. EXS 101, 133–164.

Wan, S., Ma, M., Lv, L., Qian, L., Xu, S., Xue, Y., Ma, Z., 2014. Selective capture of thallium(I) ion from aqueous solutions by amorphous hydrous manganese dioxide. Chem. Eng. J. 239, 200–206.

Webster, J.G., Swedlund, P.J., Webster, K.S., 1998. Trace metal adsorption onto an acid mine drainage iron (III) oxy hydroxy sulfate. Environ. Sci. Technol. 32 (10), 1361–1368.

WHO, 2017. Guidelines for Drinking-Water Quality: Fourth edition Incorporating the First Addendum. World Health Organization, Geneva.

Yu, J.-Y., Heo, B., Cho, J.-P., Chang, H.-W., 1999. Apparent solubilities of schwertmannite and ferrihydrite in natural stream waters polluted by mine drainage. Geochim. Cosmochim. Acta 63, 3407–3416.

Zhu, Y., Balke, K.D., 2008. Groundwater protection: what can we learn from Germany? J Zhejiang Univ Sci B 9 (3), 227–231.